Polarizabilities of Pb^{2+} and Pb^{4+} and ionization energies of Pb^{+} and Pb^{3+} from spectroscopy of high-L Rydberg states of Pb^{+} and Pb^{3+}

M. E. Hanni, Julie A. Keele, and S. R. Lundeen
Department of Physics, Colorado State University, Fort Collins, Colorado 80523, USA

C. W. Fehrenbach
J. R. Macdonald Laboratory, Kansas State University, Manhattan, Kansas 66506, USA

W. G. Sturrus
Department of Physics, Youngstown State University, Youngstown, Ohio 44555, USA

(Received 10 February 2010; published 16 April 2010)

The binding energies of high-L Rydberg levels of Pb^{+} with $n = 19$ or 20 and $6 \leqslant L \leqslant 10$ were measured with resonant excitation Stark ionization spectroscopy (RESIS). When combined with previous measurements of members of the nh Rydberg series in Pb^{+}, and analyzed with the long-range polarization model, these determined the polarizability of the $5d^{10}6s^2$ ground state of Pb^{2+} to be $\alpha_d = 13.62(8)$ a.u. This value is substantially larger than the estimate published recently based on the measured lifetime of the $6s6p^1P_1$ resonance level of Pb^{2+}, 7.9(6) a.u. The difference is mostly due to the polarizability of Pb^{4+}, the $5d^{10}$ core of the Pb^{2+} ion. This was established by observation of resolved fine structure in the excitation of $n = 39$, high-L Rydberg levels of Pb^{3+}, using the same RESIS technique. Analysis of this spectra determined the polarizability of Pb^{4+} to be $\alpha_d = 3.61(4)$ a.u. Reanalysis of optical spectra of nh and ng levels in Pb^{+} and Pb^{3+} in view of the polarizabilities determined in the RESIS studies indicates revised ionization energies of both ions, $E_I(Pb^{+}) = 121245.28(6)\ cm^{-1}$ and $E_I(Pb^{3+}) = 341\,435.1(8)\ cm^{-1}$.

DOI: 10.1103/PhysRevA.81.042512 PACS number(s): 32.30.Bv, 32.10.Dk, 32.10.Hq, 32.10.Fn

I. INTRODUCTION

The interaction of atoms and ions with external electric fields is usually dominated by the response of the valence electrons to the field, with any electrons in closed shells remaining relatively "frozen." This view becomes less valid for heavier atoms, where the "core polarizability" becomes increasingly important, and accurate calculations of atomic polarizabilities become correspondingly more challenging. The Pb^{2+} ion is a good example of this trend. Its ground state is a closed-shell $5d^{10}6s^2 1S_0$ state in the Hg-like isoelectronic sequence. The valence polarizability due to excitation of the $6s$ electrons can be estimated from the measured lifetime of the $6s6p^1P_1$ resonance state, using the oscillator strength sum rules to set limits on possible contributions from higher excited states. This is exactly what was done in 2008 by Reshetnikov *et al.* [1], who inferred a polarizability of 7.8(6) a.u. from the 0.380(21)-ns measured lifetime of the $6s6p^1P_1$ level [2]. This result differed by almost a factor of 2 from a previous determination of the polarizability of Pb^{2+}, obtained by analysis of six members of the ng Rydberg series of Pb^{+} that determined $\alpha_d = 13.38(2)$ a.u. [3]. The discrepancy between these two results provided the motivation for the present study. The polarizability of positive ions can be determined by observation of the fine-structure pattern in nonpenetrating Rydberg levels bound to the ion in question. The spectroscopy of these high-L levels can be conveniently studied by using the resonant excitation Stark ionization spectroscopy (RESIS) method [4], which can be used to study these fine-structure patterns both in neutral atoms and in Rydberg ions with a wide range of net charges. In this article, the RESIS method was used to study high-L Rydberg fine-structure patterns in both Pb^{+} and Pb^{3+}, determining the dipole polarizabilities of both core ions, Pb^{2+} and Pb^{4+}. The results supported the larger estimate of the Pb^{2+} polarizability obtained previously by analysis of the ng Rydberg series in Pb^{+} [3] and confirmed that the Pb^{4+} core contributes about 25% of this total. This illustrates the increasing importance of closed-shell polarizabilities in heavy ions. The precise knowledge of very high L fine-structure energies in the Pb^{+} and Pb^{3+} ions also allowed the redetermination of the ionization potentials in both ions from existing optical spectroscopy.

II. EXPERIMENT

This experiment is possible because of the installation of a new 14-GHz permanent magnet electron cyclotron resonance (ECR) ion source at the J. R. Macdonald Laboratory of Kansas State University. This source produces multiply charged ion beams by sputtering solid samples and easily generates either of the ion beams (Pb^{2+} or Pb^{4+}) needed for this study. The two RESIS studies are similar in most respects, so the Pb^{+} study will be described initially. The apparatus used for this study is shown schematically in Fig. 1. Beams of multiply charged Pb ions are extracted from the ion source, accelerated through a 10-kV potential, focused with a quadrupole doublet lens, and charge analyzed by a 20° bending magnet. The Pb^{2+} ion beam selected by the magnet then passes through a second quadrupole doublet lens and through a 2-mm aperture into the remainder of the RESIS apparatus. The source, charge selection process, and ion optics are shown as a block at (1) in Fig. 1. The Pb^{2+} beam first passes through a dense Rydberg target where a fraction of the ions capture a single electron to form highly excited Rydberg Pb^{+} ions. The Rydberg target, at (2) in Fig. 1, is formed from a thermal beam of Rb atoms

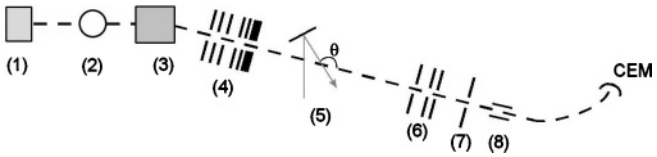

FIG. 1. Block schematic of the RESIS apparatus used for this study. The fast ion beams are created by an ECR source, accelerated through a 10-kV potential, and passed into a 20° magnet at (1) where the charge of the beam is selected. At (2) the fast ion beam intersects the Rydberg target, and resonant charge capture results in a beam of highly excited Rydberg ions. The Rydberg ion beam is selected from the residual ion beam by using another charge selection magnet at (3) in the diagram. The Rydberg beam then passes trough two Einzel lenses at (4). These lenses ionize any weakly bound Rydberg states and focus the beam for transport through the rest of the apparatus. At (5) the Rydberg beam intersects a Doppler-tuned CO_2 laser. The laser selectively excites high angular momentum states from a lower-n Rydberg level to a higher n. The ions with highly excited Rydberg states are then ionized and energy tagged at (6), focused by a small lens electrode at (7), and steered into a CEM at (8) that monitors the Stark ionization current.

that are excited to the $12F_{7/2}$ state via the $5P_{3/2}$ and $4D_{5/2}$ states, using three cw lasers [5]. The transitions from the $5S_{1/2}$ ground state to the $5P_{3/2}$ excited state and from the $5P_{3/2}$ to the $4D_{5/2}$ excited state of Rb are driven with diode lasers. The final transition from the $4D_{5/2}$ to the $12F_{7/2}$ final state is driven using a tunable Ti:sapphire laser. The $12F$ target was chosen to maximize the capture into Rydberg levels bound to the incident Pb^{2+} ion by approximately one CO_2 laser photon [6]. The fast Pb^+ Rydberg ions as well as any remaining Pb^{2+} ions enter another 15° analyzing magnet at (3) in Fig. 1. The magnetic field at (3) is tuned to steer only the Pb^+ ions through the rest of the apparatus. The Rydberg ion beam then enters a dual einzel lens assembly at (4). The first einzel lens in the assembly is held at −7.6 kv, producing a ∼2700 V/cm field sufficient to ionize any Pb^+ ions that have captured an electron into a level with $n \geqslant 44$. The second einzel lens is held at −1.0 kv, producing a ∼1250 V/cm field, sufficient to diabatically Stark mix the L populations of the $n = 19$ and 20 levels of Pb^+. This is done to transfer population from the long-lived very high L levels to the high-L levels that might be resolved in the RESIS spectra. Immediately following the second einzel lens is the laser interaction region (LIR) at (5) in Fig. 1. In the LIR a fixed-frequency CO_2 laser reflects off a rotatable mirror and intersects the fast Rydberg beam at a variable angle $\theta_{\rm Int}$. The laser line is selected to be close to a possible upward transition between Rydberg levels of Pb^+. Table I lists the transitions, velocities, and CO_2 laser frequencies used in this study of Rydberg levels of Pb^+ and also includes the transition in Pb^{3+} which will be described later. The frequency of the laser, as seen from the rest frame of the ion beam, is Doppler-tuned according to

$$\upsilon_L' = \frac{\upsilon_L}{\sqrt{1-\beta^2}}(1+\beta\cos\theta_{\rm Int}), \qquad (1)$$

where ν_L is the frequency of the CO_2 laser and β is the velocity of the ion beam divided by c. The laser selectively excites a particular n,L fine-structure level to a much higher level that was previously emptied by the first einzel lens element. The

TABLE I. Specific RESIS transitions used in this study. The first column lists the Rydberg ion, and the second column specifies the initial and final n of the RESIS transition. The third column lists the ion velocity, the fourth column the CO_2 laser frequency, and fifth column the hydrogenic frequency for the transition. The sixth column is the perpendicular angle of the CO_2 laser.

	Transition observed n–n'	v/c	CO_2 laser frequency (cm^{-1})	E_0 (cm^{-1})	$\theta_{\rm Perp}$ (deg)
Pb^+	20–52	0.0 004 548(5)	934.8945	935.0374	1.12(5)
	19–52	0.0 004 548(5)	1053.9235	1053.5898	1.08(3)
Pb^{3+}	39–93	0.0 006 432(6)	951.1923	951.3619	1.12(5)

highly excited Rydberg ions are then Stark ionized at (6) and energy tagged to distinguish them from other ions formed by background collisions with the residual gas in the system or through other processes. The lens at (7) in Fig. 1 then focuses the remaining beam through the steering plates at (8) that direct the beam into the channel electron multiplier (CEM) at the end of the apparatus. The CEM current synchronous with chopping of the CO_2 laser is the RESIS signal. When measured as a function of the variable angle of intersection between that laser and the fast ion beam, a strong signal is observed when the Doppler-tuned laser frequency is resonant with a transition upward from a state that is too low in n to be ionized in the detector into a higher state that will be ionized in the detector. An example of the resulting RESIS excitation spectra for Pb^+ can be seen in Fig. 2. The largest signal in Fig. 2 corresponds to excitation of very high L levels whose binding energies are too close to hydrogenic to be resolved. At slightly higher energies, however, lower L levels with successively larger binding energies are observed. The procedure used to identify the resolved signals is described in Sec. III A. The x axis in the figure is the angle, $\theta_{\rm Obs}$, recorded by the computer

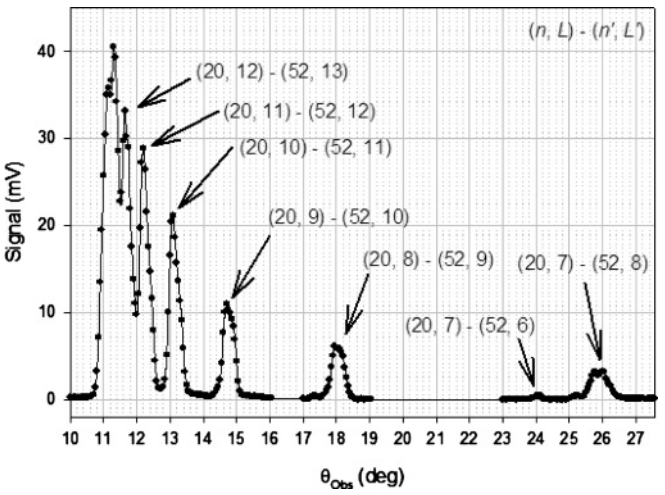

FIG. 2. RESIS spectrum of 20–52 transitions in Pb^+ showing resolved fine-structure transitions involving high-L Rydberg levels. The x axis represents the rotation angle of the mirror as recorded by the computer. The transitions representing excitation of $n = 20$, $L = 11,12$ levels were not used in the analysis since they were not fully resolved.

TABLE II. Resolved RESIS transitions observed in this study. Column 1 lists the ion, column 2 lists the transition observed, and column 3 gives the number of independent observations of that transition. Column 4 lists the average fitted center angle of the transition when fit to a Gaussian. The error reported is the larger of the internal or external error. Column 5 lists the intersection angle of the transition and column 6 lists the energy difference of the observed transition from the hydrogenic energy of the transition. The error reported on the measurements in column 6 represents the combined error in the intersection angle, the velocity of the ion beam, and θ_{Perp}.

	Transition (n,L)–(n',L')	Number of observations	θ_{Obs} (deg)	θ_{Int} (deg)	ΔE_{Obs} (MHz)
Pb^{+}	(20,10)–(52,11)	4	13.131(5)	65.98(10)	905(21)
	(20,9)–(52,10)	4	14.774(5)	62.69(10)	1564(21)
	(20,8)–(52,9)	4	18.047(10)	56.15(10)	2816(20)
	(20,7)–(52,8)	4	25.90(2)	40.44(11)	5417(18)
	(20,7)–(52,6)	4	24.06(11)	44.1(2)	4870(39)
	(19,6)–(52,7)	4	7.439(17)	77.28(7)	13 168(17)
Pb^{3+}	(39,10)–(93,11)	4	10.827(8)	70.59(10)	1010(31)
	(39,9)–(93,10)	4	12.145(11)	67.95(10)	1801(31)
	(39,8)–(93,9)	4	14.95(2)	62.35(11)	3427(32)

controlling the mirror rotation. This is related to the actual intersection angle by an arbitrary offset. The angle θ_{Int} can be determined from θ_{Obs} by

$$\theta_{\text{Int}} = 90^{\circ} - 2(\theta_{\text{Obs}} - \theta_{\text{Perp}}), \tag{2}$$

where θ_{Perp} is the angle at which the reflected CO_2 laser is exactly perpendicular to the ion beam velocity. Column 3 of Table II lists the average observed angle for the resolved transitions in the RESIS excitation spectrum for the Pb^{+} ion. The intersection angles for the same transitions are shown in column 4. The energy difference between the nonrelativistic hydrogenic frequency of the transition being studied and the Doppler-tuned CO_2 laser frequency can be found by

$$\Delta E_{\text{Obs}} = \upsilon_L' - \nu_0, \tag{3}$$

where υ_0 is determined by

$$\upsilon_0 = \frac{\text{Ryd}_M}{h} q^2 \left(\frac{1}{n^2} - \frac{1}{n'^2} \right). \tag{4}$$

The energy differences of the observed transitions are reported in the last column of Table II.

Calculation of the Doppler-tuned laser frequency υ_L', and therefore ΔE_{Obs}, depends upon knowledge of the beam velocity, β, and knowledge of θ_{Perp}. The beam velocity was determined by a calibrated voltage measurement of the acceleration potential. The value of θ_{Perp} was determined by observing fine-structure patterns on opposite sides of θ_{Perp}. The values appropriate for different data sets are shown in the last column of Table I.

III. ANALYSIS AND RESULTS

A. Line identifications

The Pb^{+} excitation spectrum of Fig. 2 shows at least six fully resolved transitions occurring at slightly higher frequencies than the unperturbed hydrogenic transition frequency. The sequence of frequency differences from hydrogenic frequency, shown in the last column of Table II, is well defined and systematic. The main peaks are due to excitation of successively lower angular momentum levels of $n = 20$ moving to the right on the x axis. Since, in lowest order, the fine-structure energies are expected to be proportional to the expectation value of the inverse fourth power of r, the lines were identified by choosing the specific L values that make the entire sequence most nearly proportional to the sequence of expectation values of r^{-4}. With the identifications shown on Fig. 2, this ratio changes by less than 5% across the range of transitions observed. Alternate identifications of the lines, by increasing or decreasing the L value by one unit, result in a change in this ratio by at least 30% across the range of lines. This identification is also supported by comparison to the positions of nh and ng Rydberg levels reported elsewhere, as discussed in the following.

B. Theoretical model

The effective potential model that describes the fine-structure pattern for nonpenetrating high-L Rydberg states with S-state cores has been used for many years [7]. In recent years, it has been substantially extended and given a much firmer theoretical foundation by Drachman [8]. Since Pb^{2+} has a $^1S_0$ ground state, the effective potential describing Rydberg levels of Pb^{+} contains only scalar terms and is of the form

$$V_{\text{eff}} = -\frac{\alpha_d}{2r^4} - \frac{(\alpha_q - 6\beta_d)}{2r^6} + \cdots, \tag{5}$$

where the coefficients are properties of the core ion: α_d, the total dipole polarizability; α_q, the quadrupole polarizability; and β_d, the nonadiabatic dipole polarizability. The energy levels can then be expressed in terms of V_{eff} by

$$E(nL) = E^0(n) + E^{\text{rel}}(nL) + E^{[1]}(nL) + E^{[2]}(nL), \tag{6}$$

where $E^0(n)$ is the zeroth-order energy of a Rydberg level with principal quantum number n. The second term, E^{rel}, is a relativistic correction due to the "p^4" contributions to kinetic energy and is given by

$$E^{\text{rel}} = \frac{\alpha^2 q^4}{2n^4} \left(\frac{3}{4} - \frac{n}{L + \frac{1}{2}} \right). \tag{7}$$

The third term, $E^{[1]}(nL)$, is the expectation value of V_{eff} and is by far the most significant contribution to the fine-structure pattern. The fourth term, $E^{[2]}$, comes from application of V_{eff} in second order and has been calculated analytically by Drake and Swainson [9] in the approximation that only the term proportional to α_d^2 is significant.

C. Determination of core parameters

The difference in frequency between a specific RESIS transition and the corresponding hydrogenic frequency, ΔE_{Obs}, is due to the fine-structure energies of both upper $(n'L')$ and lower (nL) levels of the transition, but the lower level's fine-structure energy is dominant. ΔE_{Obs} can be expressed as

$$\Delta E_{\text{Obs}} = [E^{[1]}(n'L') + E^{[2]}(n'L') + E^{\text{rel}}(n'L')] - [E^{[1]}(nL) + E^{[2]}(nL) + E^{\text{rel}}(nL)]. \tag{8}$$

In order to compare with the effective potential model and determine the core parameters, the dominant contribution due to the difference in $E^{[1]}$ in the upper and lower levels is isolated by calculating and subtracting the small corrections from $E^{\rm rel}$ and $E^{[2]}$, giving

$$\Delta E^{[1]} \equiv \Delta E_{\rm Obs} - \Delta E^{[2]}(nL) - \Delta E^{\rm rel}(nL) - \Delta E_{\rm Stark}(n'L'). \tag{9}$$

The term $\Delta E_{\rm Stark}$ represents perturbation of the upper state position by stray electric fields in the LIR. The magnitude of the stray electric field in the LIR region was estimated from the observed widths of the RESIS lines, giving a result that ranged from 0.025 to 0.055 V/cm. Simulations including the zero-field fine structure of the upper state and fields of these magnitudes showed little or no shift in the line positions. For completeness, the estimated shifts are shown in column 6 of Table III.

A scaled plot of the corrected first-order energies yields an estimate of the core ion's polarizability.

$$\frac{\Delta E^{[1]}}{\Delta\langle r^{-4}\rangle} = \frac{\alpha_d}{2} + \frac{(\alpha_Q - 6\beta_d)}{2}\frac{\Delta\langle r^{-6}\rangle}{\Delta\langle r^{-4}\rangle} + \cdots, \tag{10}$$

where

$$\Delta\langle r^{-4}\rangle \equiv [\langle r^{-4}\rangle_{nL} - \langle r^{-4}\rangle_{n'L'}], \tag{11}$$

etc. and the radial expectation values are taken to be the hydrogenic values [10] corrected for the finite mass of the Pb^{2+} core. The plot of the scaled values of $\Delta E^{[1]}$ for Pb^{+} is shown in Fig. 3 as solid circles. The position of points along the x axis is determined by the ratio

$$\frac{\Delta\langle r^{-6}\rangle}{\Delta\langle r^{-4}\rangle}$$

TABLE III. List of the small corrections applied to isolate the first-order polarization energy differences from the measured frequency offsets between the several resolved RESIS transitions and the respective hydrogenic transition frequencies. Columns 1, 2, and 3 are reproduced from Table II for reference. Columns 4 and 5 list the small contributions to the measured offsets due to relativistic and second-order energies. Column 6 is an estimate of the contribution to the offset from Stark shifts of the upper state due to the presence of a 25 mV/cm field. A larger 55 mV/cm field was present during the observation of the (19,6)–(52,7) transition. The final column lists $\Delta E^{[1]}$, the difference between the first-order polarization energies of the two levels involved in the RESIS transition.

	Transition (n,L)–(n',L')	$\Delta E_{\rm Obs}$ (MHz)	$\Delta E^{\rm rel}$ (MHz)	$\Delta E^{[2]}$ (MHz)	$\Delta E_{\rm Stark}$ (MHz)	$\Delta E^{[1]}$ (MHz)
Pb^{+}	(20,10)–(52,11)	905(21)	19	0	0	886(21)
	(20,9)–(52,10)	1564(21)	22	1	+1	1540(21)
	(20,8)–(52,9)	2816(20)	26	3	+1	2786(20)
	(20,7)–(52,8)	5417(18)	32	12	0	5373(18)
	(20,7)–(52,6)	4870(39)	31	9	−2	4832(39)
	(19,6)–(52,7)	13 168(17)	44	71	−10	13 063(17)
Pb^{3+}	(39,9)–(93,10)	1010(31)	60	1	0	949(31)
	(39,8)–(93,9)	1801(31)	69	2	0	1730(31)
	(39,7)–(93,8)	3427(32)	80	8	0	3339(32)

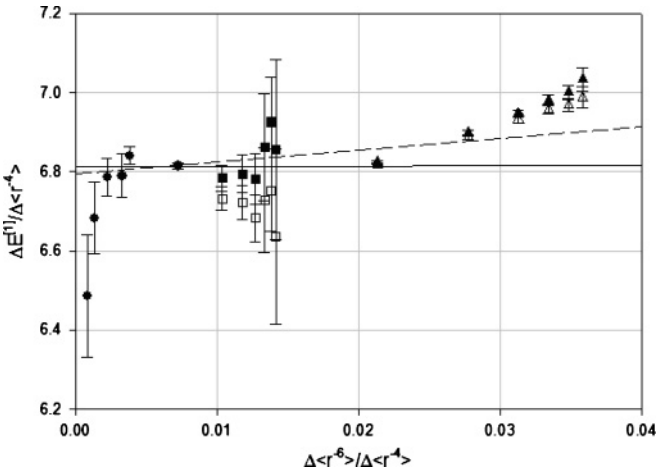

FIG. 3. Plot of the scaled first-order polarization energies in Pb^{+}. The solid circles represent the RESIS data of this study. The squares represent the nh levels [3] and the triangles the ng levels [11]. The open squares and open triangles assume the Pb^{+} ionization energy of 121 245.14(5) cm^{-1}, while the solid squares and triangles assume the value of $E_{\rm I}$ indicated by a fit of the RESIS and nh data, 121 245.28(6) cm^{-1}. The vertical axis represents the ratio of the first-order polarization energy to the expectation value of r^{-4}, as described in the text. The horizontal axis represents the ratio of the expectation value of r^{-6} to that of r^{-4}. The dashed line represents a fit of the RESIS data alone to the effective potential model. The solid line represents a fit of the RESIS data and the nh levels. The ng levels were not used in either fit, although they appear to lie on a smooth curve with the higher L data. Energies and lengths are in atomic units.

for a particular transition. The dashed line in Fig. 3 is a linear fit to RESIS data, the solid circles. The fitted slope and intercept are shown in Table IV. The intercept implies a polarizability of 13.58(10) for Pb^{2+}, nearly consistent with the value of 13.38(2) reported from analysis of the ng Rydberg series by Ross *et al.* [3].

It is of interest to reexamine the ng and nh Rydberg series positions reported by Wood *et al.* [11] and Ross *et al.* [3], in light of this new determination of α_d. The reported positions represent the excitation energies from the ground state of Pb^{+}, so the fine-structure energies can be inferred only with an assumption of the ionization energy, $E_{\rm I}$, according to

$$E_{\rm Obs} = E_I + E^0(n) + E^{\rm rel}(nL) + E^{[1]}(nL) + E^{[2]}(nL). \tag{12}$$

The last term, $E^{[2]}$, represents the second-order contribution to the energy due to the polarization potential. This was not included in the analysis of Ross *et al.* [3], but has since been firmly established theoretically [8,9]. Starting with the

TABLE IV. Parameters determined from the fits of the Pb^{+} Rydberg fine-structure data in Fig. 3 to the effective potential model.

Data used in the fit	B_4 (a.u.)	B_6 (a.u.)	$E_{\rm I}$ (cm^{-1})
RESIS	6.79(5)	3(8)	...
RESIS and nh[a]	6.81(4)	0(6)	121 245.28(6)

[a]Ross *et al.* [3].

TABLE V. The measured energy levels of the *ng* [11] and *nh* [3] Rydberg levels of Pb^+ relative to the ground state of that ion are shown in column 2. Column 3 is the nonrelativistic hydrogenic energy of a Rydberg level with quantum number *n*, and column 4 is the relativistic energy contribution to that energy. Column 5 gives the second-order polarization energy, assuming a polarizability of 13.38 a.u. Column 6 is the inferred first-order polarization energy assuming the ionization energy of Pb^+ is 121 245.14(5) cm^{-1}.

nL	E_{Obs} (cm^{-1})	E^0 (cm^{-1})	$E^{Rel}(nL)$ (cm^{-1})	$E^{[2]}(nL)$ (cm^{-1})	$E^{[1]}(n,L)$ (cm^{-1})
$5g$[??]	103 560.95(2)	−17 557.92	−0.06	−4.62	−121.59(5)
$6g$[a]	108 969.62(2)	−12 193.00	−0.04	−3.49	−78.99(5)
$7g$[a]	112 231.40(3)	−8958.12	−0.04	−2.50	−53.08(6)
$8g$[a]	114 347.74(2)	−6858.56	−0.03	−1.80	−37.01(5)
$9g$[a]	115 798.01(3)	−5419.11	−0.02	−1.33	−26.67(6)
$10g$[a]	116 834.82(6)	−4389.48	−0.01	−1.00	−19.83(8)
$7h$[b]	112 269.73(6)	−8958.12	−0.03	−0.21	−17.05(8)
$8h$[b]	114 374.31(6)	−6858.56	−0.02	−0.16	−12.09(8)
$9h$[b]	115 817.12(6)	−5419.11	−0.02	−0.12	−8.77(8)
$10h$[b]	116 848.95(12)	−4389.48	−0.01	−0.09	−6.61(13)
$11h$[b]	117 612.31(6)	−3627.67	−0.01	−0.07	−5.08(8)
$12h$[b]	118 192.92(12)	−3048.25	−0.01	−0.06	−3.90(13)

[a]Wood *et al.* [11].
[b]Ross *et al.* [3].

ionization energy reported by Ross, $E_I = 121\,245.14(5)\,cm^{-1}$, $E^{[1]}(nL)$ for each observed level can be calculated from Eq. (12), with the results listed in Table V. Also shown in Table V are the contributions of each of the other terms in Eq. (12). Notice that the contribution of $E^{[2]}$ amounts to about 4% of $E^{[1]}$ for the *ng* series and about 1% of $E^{[1]}$ for the *nh* series. In view of this, the 1.6% agreement between the RESIS result for α_d and the earlier report based on the *ng* series must be considered to be fortuitous.

The inferred values of $E^{[1]}$ for the *nh* and *ng* levels of Pb^+ can be added to Fig. 3 by considering the frequency offset that would occur if each were excited to an upper state with hydrogenic energy (i.e. $\Delta E_{Obs} = -E^{[1]}$). For this hypothetical transition, $\Delta\langle r^{-4}\rangle = \langle r^{-4}\rangle$ and $\Delta\langle r^{-6}\rangle = \langle r^{-6}\rangle$. The appropriate points would be found by dividing $-E^{[1]}$ by the expectation value of $\langle r^{-4}\rangle$ and plotting versus the ratio $\langle r^{-6}\rangle/\langle r^{-4}\rangle$. According to the polarization model, the resulting plot should have the same intercept and slope as the earlier plot including only the RESIS data. The scaled energies of the *nh* Rydberg levels are shown in Fig. 3 as open squares, while the scaled energies of the *n*g Rydberg levels are shown as open triangles. All of the scaled points lie within a range of ±4%, supporting the line identifications in the RESIS spectrum of Fig. 2. The points due to the *ng* series do appear to lie in a straight line, but neither the slope nor the intercept of this line is in agreement with the RESIS data, or for that matter with the *nh* data. The disagreement between the two series was noted and discussed by Ross *et al.* [3] and it was suggested that this could be due to the influence of core penetration. The effects of core penetration are difficult to estimate precisely but are certain to be more significant in the $L = 4$ series than in the $L = 5$ series or in the even higher *L* levels included in the RESIS data. The presence of significant core penetration effects on the *ng* term energies would invalidate the application of the effective potential model, which explicitly excludes such effects. The scaled fine-structure energies from the *nh* series are in much closer agreement with the fine-structure intervals reported here, and the agreement can be further improved by adjustment of the ionization energy. An upward adjustment of +0.14(6) cm^{-1} modifies the plotted points from both the *nh* and *ng* series to the solid squares and triangles in Fig. 3. This choice of E_I results from a least-square fit of both the RESIS data and the *nh* series data to the form of Eq. (11) but also allowing E_I to vary, leading to the solid line in Fig. 3 and the fitted parameters listed in Table IV. The value of α_d implied by this fit is 13.62(8) a.u. and is completely consistent with the value found from the RESIS data alone. Both fits find a small slope, as indicated in Table IV. The adjustment to E_I has only a minor effect on the scaled energies from the *ng* series since their fine-structure energies are much larger. The corrected points from the *ng* positions, shown as solid triangles in Fig. 3, appear to lie on a smooth curve with the points derived from the RESIS data and the *nh* series, but not on a straight line. The deviation of the *ng* points could be due to core penetration effects, as speculated by Ross *et al.* [3], or it could be due to higher order contributions to the effective potential.

The final value for the Pb^{2+} polarizability, 13.62(8) a.u., is much larger than the value suggested by Reshetnikov *et al.* [1] from consideration of the $6s6p\,^1P_1$ lifetime, 7.8(6) a.u. The difference is much too great to be due to an error in the measured lifetime. Another possibility is that the polarizability of the $5d^{10}$ core of the Pb^{2+} ion (i.e. the Pb^{4+} ion) contributes a substantial fraction of the total Pb^{2+} polarizability. To investigate this experimentally, the RESIS method was used to examine the 39–93 excitation spectrum of Pb^{3+}. This was easy to accomplish by simply selecting the Pb^{4+} beam instead of the Pb^{2+} beam at the initial charge selection magnet. If the polarizability of the Pb^{4+} ion is small, this spectrum would not be expected to reveal any resolved fine structure. Table I gives details of the 39–93 RESIS transition. The observed spectrum, shown in Fig. 4, reveals at least three well-resolved excitations, and this by itself indicates a substantial polarizability. The details of the resolved transitions and the inferred fine-structure energies are shown in Tables II and III. By using the line identifications of Fig. 4, a polarization plot analogous to Fig. 3 can be constructed, and this is shown in Fig. 5. A fit of the RESIS data, shown by solid circles, gives the intercept and slope shown in Table VI. The line identifications shown in Fig. 4 were confirmed by comparison with optical spectroscopy of the 5*g* and 6*h*–8*h* levels of Pb^{3+} [12]. The optical data can be included on Fig. 5, as on Fig. 3, by initially assuming the previously accepted ionization potential,

TABLE VI. Parameters determined from the fits of the Pb^{3+} Rydberg fine-structure data in Fig. 5 to the effective potential model.

	B_4(a.u.)	B_6 (a.u.)	E_I (cm^{-1})
RESIS	1.80(6)	7(4)	. . .
RESIS including 5*g* and 6*h*–8*h*[a]	1.806(18)	6.9(2)	341 435.1(8)

[a]Crawford *et al.* [12].

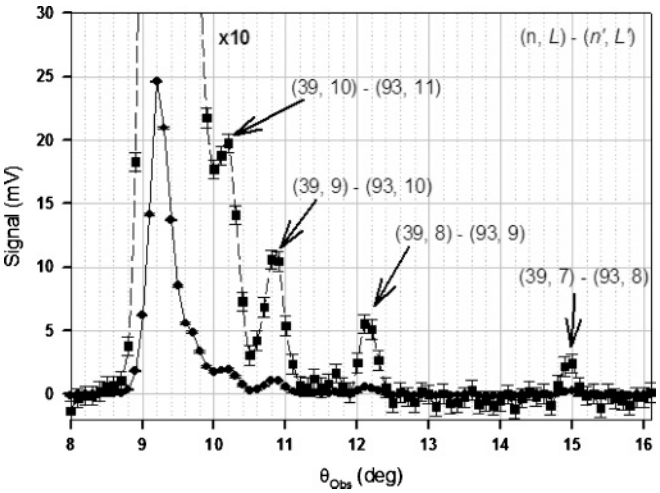

FIG. 4. RESIS spectrum of 39–93 transitions in Pb^{3+} showing resolved fine-structure transitions, as indicated. The square points connected with a dashed line have been multiplied by a factor of 10 for clarity in viewing the resolved fine-structure transitions. The x axis represents the rotation angle of the mirror as recorded by the computer.

341 350 cm^{-1}, [12]. The details of these energy levels are shown in Table VII, which is analogous to Table V. This results in the open squares and open triangles on Fig. 5. The nh positions are obviously discrepant, and this is not surprising given that they were assumed to be hydrogenic in order to derive the ionization potential [12]. A much better estimate of the ionization potential can be found by fitting all the data in Fig. 5 to the form of Eq. (11), but allowing the ionization

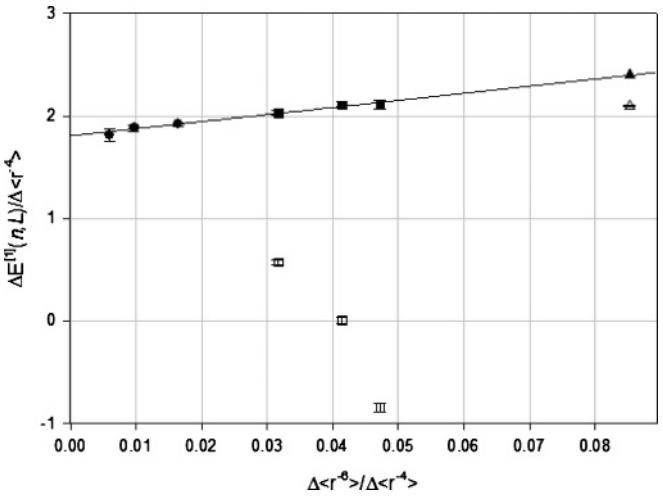

FIG. 5. Plot of the scaled first-order polarization energies in Pb^{3+}. The solid circles represent the RESIS data of this study. The squares and triangles represent the nh and $5g$ levels [12]. The open squares and open triangles assume the Pb^{3+} ionization energy of 341 350 cm^{-1}, while the solid squares and triangles assume the value of E_I indicated by a fit of the RESIS, nh, and $5g$ data, 341 435.2(8) cm^{-1}. The vertical axis represents the ratio of the first-order polarization energy to the expectation value of r^{-4}, as described in the text. The horizontal axis represents the ratio of the expectation value of r^{-6} to that of r^{-4}. The solid line represents a fit of all the data to the linear form predicted by the polarization model. Energies and lengths are in atomic units.

TABLE VII. The measured energy levels of the $5g$ and $6h$–$8h$ Rydberg levels of Pb^{3+} relative to the ground state of that ion are shown in column 2. Column 3 is the nonrelativistic hydrogenic energy of a Rydberg level with quantum number n, and column 4 is the relativistic energy contribution to that energy. Column 5 gives the second-order polarization energy, assuming a polarizability of 3.63 a.u. Column 6 is the inferred first-order polarization energy assuming the ionization energy of Pb^{3+} is 341 350 cm^{-1}.

nL	E_{Obs} (cm^{-1})	E^0 (cm^{-1})	$E^{Rel}(nL)$ (cm^{-1})	$E^{[2]}(nL)$ (cm^{-1})	$E^{[1]}(n,L)$ (cm^{-1})
$5g$[a]	270 497(1)	−70 231.7	−0.9	−21.9	−598.5(1.0)
$6h$[a]	292 543(1)	−48 772.0	−0.4	−1.2	−33.4(1.0)
$7h$[a]	305 516(1)	−35 832.5	−0.3	−1.0	−0.2(1.0)
$8h$[a]	313 939(1)	−27 434.3	−0.3	−0.8	24.4(1.0)

[a]Crawford *et al.* [12].

energy to vary. This results in a significant revision of E_I, and the recalculated scaled positions for the nh and $5g$ levels shown by the solid squares and solid triangles in Fig. 5. The fit parameters returned by this fit are shown in Table VI. The polarizability of Pb^{4+} is determined to be 3.61(4) a.u. and the ionization energy of Pb^{3+} is found to be 341 435.1(8) cm^{-1}.

IV. DISCUSSION

Table VIII summarizes the quantities determined in this study, dipole polarizabilities of Pb^{2+} and Pb^{4+} and ionization energies of Pb^{+} and Pb^{3+}. These results depend both on the RESIS spectroscopy reported here and on previous optical spectroscopy of ng and nh levels. The RESIS data determine precise values of the dipole polarizabilities, but the optical spectroscopy is necessary to confirm the identification of the RESIS lines and to determine the ionization energies. The measured polarizabilities of Pb^{2+} and Pb^{4+} illustrate the importance of the core polarizability in heavy ions. In the case of Pb^{2+}, the $5d^{10}$ core contributes more than 25% of the total polarizability. If the total polarizability is simply the sum of the core and valence polarizabilities, as usually assumed, then the Pb^{2+} valence polarizability determined

TABLE VIII. Summary of the ion properties determined in this study. Column 1 lists the ion, and column 2 gives the property determined. Column 3 provides the value for the property determined in this study and column 4 provides the past determination for reference. The valence polarizability of Pb^{2+}, α_d^V, was computed by subtracting the polarizabilities of Pb^{2+} and Pb^{4+}.

Ion	Property	Present determination	Previous determination
Pb^{+}	E_I	121 245.28(6) cm^{-1}	121 245.14(5) cm^{-1}[a]
Pb^{2+}	α_d	13.62(8) a.u.	13.38(2) a.u.[a]
Pb^{2+}	α_d^V	10.01(9) a.u.	7.8(6) a.u.[b]
Pb^{3+}	E_I	341 435.1(8) cm^{-1}	341 350 cm^{-1}[c]
Pb^{4+}	α_d	3.61(4) a.u.	...

[a]Ross *et al.* [3].
[b]Reshetnikov *et al.* [1].
[c]Crawford *et al.* [12].

in this study, 10.01(9) a.u., is in poor agreement with the valence polarizability reported by Reshetnikov *et al.* [1], 7.8(6) a.u. This may call into question the usual assumption. The Pb^{4+} polarizability determined here is consistent with the trend of calculated polarizabilities for the analogous $3d^{10}$ and $4d^{10}$ ions, Ge^{4+} and Sn^{4+}. In these cases, Johnson *et al.* calculated 0.76 and 2.26 a.u. respectively [13]. We know of no direct calculations for either Pb^{2+} or Pb^{4+}. The ionization energy determined for Pb^{+} differs only slightly from the previously accepted value, but the ionization energy for Pb^{3+} is substantially different from the previously accepted value.

ACKNOWLEDGMENTS

This work is supported by the Chemical Sciences, Geosciences, and Biosciences Division of the Office of Basic Energy Sciences, Office of Science, US Department of Energy. The experiments were conducted at J. R. Macdonald Laboratory of Kansas State University.

[1] N. Reshetnikov, L. J. Curtis, M. S. Brown, and R. E. Irving, Phys. Scr. **77**, 015301 (2008).
[2] L. J. Curtis *et al.*, Phys. Rev. A **63**, 042502 (2001).
[3] C. B. Ross, D. R. Wood, and P. S. Scholl, J. Opt. Soc. Am. **66**, 36 (1976).
[4] S. R. Lundeen, in *Advances in Atomic, Molecular, and Optical Physics*, edited by Chun C. Lin and Paul Berman (Academic Press, New York, 2005), Vol. 52, pp. 161–208.
[5] C. W. Fehrenbach, S. R. Lundeen, and O. L. Weaver, Phys. Rev. A **51**, R910 (1995).
[6] D. S. Fisher, S. R. Lundeen, C. W. Fehrenbach, and B. D. DePaola, Phys. Rev. A **63**, 052712 (2001)
[7] B. Edlén, *Handbuch der Physik XXVII*, edited by S. Flügge (Springer-Verlag, Berlin, 1964), pp. 80–220.
[8] R. J. Drachman, Phys. Rev. A **26**, 1228 (1982).
[9] G. W. F. Drake and R. A. Swainson, Phys. Rev. A **44**, 5448 (1991).
[10] K. Bockasten, Phys. Rev. A **9**, 1087 (1974).
[11] D. R. Wood, C. B. Ross, P. S. Scholl, and M. L. Hoke, J. Opt. Soc. Am. **64**, 1159 (1974).
[12] M. F. Crawford, A. B. McLay, and A. M. Crooker, Proc. R. Soc. London Ser. A **158**, 455 (1937).
[13] W. R. Johnson, D. Kolb, and K. N. Huang, At. Data Nucl. Data Tables **28**, 333 (1983).